ELSEVIER

Journal of Hazardous Materials 49 (1996) 89–101

JOURNAL OF HAZARDOUS MATERIALS

The role of aspect ratio on entrainment rates of instantaneous, axisymmetric finite volume releases of dense fluid

Pablo Huq

College of Marine Studies and Center for Applied Coastal Research, University of Delaware, Newark, DE 19716, USA

Received 17 May 1995; accepted 17 October 1995

Abstract

This article presents the results of laboratory experiments designed to discriminate the role of the initial aspect ratio (height/radius) on the dilution and entrainment rates of instantaneous releases of dense, axisymmetric finite volumes into a larger, sector-shaped volume of less dense, quiescent fluid. The effect of increasing the aspect ratio is to increase the dilution. Entrainment velocities are shown to be related to the speed of advancement of the leading edge of the intrusion and the aspect ratio. In comparison to low aspect ratio releases, high aspect ratio configurations have much greater entrainment velocities initially; subsequently, dependence of entrainment velocities upon the aspect ratio diminishes.

Keywords: Aspect ratio; Dilution; Entrainment rate; Gravity current

1. Introduction

The estimation of the dispersion of dense gases is a significant constituent in evaluating the hazard and magnitude of risk associated with accidental releases of toxic dense gases. The need for reliable concentration estimates has led to various modelling approaches. Mathematical models are still in the formative stage because of the complexities of the dispersion process. Experimental modelling approaches are attractive in that wind and water tunnel measurements permit a degree of control and repeatability which is not possible outside the laboratory. However, presently there is a discrepancy in the values of dilutions between water and wind tunnel simulations of instantaneous releases of dense gases. The theory and water tunnel experiments of Huppert and Simpson [1] and Rottman and Simpson [2] show no dilution. However, the gaseous experiments of Hall et al. [3,4], Spicer and Havens [5] and Meroney and Lohmeyer [6]

0304-3894/96/$15.00
SSDI 0304-3894(95)00147-6

show large dilutions. The contradiction may have been a result of the significant difference in molecular diffusivities. However, preliminary experiments showed that flows driven by thermal and salinity gradients in a water tunnel, which have molecular diffusivities that differ by two orders of magnitude, had similar values of dilution. The quantitative difference in the values of dilution appear to be related to variations between experiments of the aspect ratio, $h_0/2R_0$, defined to be the ratio of the initial height (h_0) to the diameter ($2R_0$) of the vessel containing the dense fluid. Consequently, the object of this article is to determine dilution rates arising from the instantaneous release of relatively dense, axisymmetric, finite volumes in water so as to discriminate the influence of the aspect ratio upon dilution.

2. Previous studies

Much of the fundamental work on gravity driven intrusions has been done by Benjamin [7] and Britter and Simpson [8–10]. Benjamin presented a theoretical investigation of the properties of steady gravity currents. Utilizing perfect fluid theory without mixing, he determined that the only non-trivial steady energy conserving solution is when the depth of the gravity current is half that of the receiving channel. Flows are possible for smaller depths, but the loss of energy at the front exceeds that available by wave radiation, so that breaking must occur. This implies the existence of an enlarged "head" at the leading edge of the intrusion; the head region is characterized by breaking, intense turbulent motions and mixing. Britter and Simpson [8] determined that the entrainment rate for such steady flows was $g' \frac{Q}{U_F^2} \approx 0.15$ where $g' = (\Delta\overline{\rho}/\overline{\rho})g$ is the reduced gravitational acceleration with $\Delta\overline{\rho}$ the density difference between the dense fluid of the gravity current and the background/ambient density $\overline{\rho}$; U_F is the propagation velocity of the head; and Q is the entrainment caused by wave breaking behind the head. Though the instantaneous release of dense fluid is not a steady flow, some features are similar — principally, the characteristic head form.

The major articles concerning the instantaneous releases of dense fluid (Fay [11], Hoult [12], Huppert and Simpson[1], Rottman and Simpson [2]). Rottman et al. [13] ignore the effects of mixing. However, the gaseous experiments of Hall [3,4], Spicer and Havens [5] and Meroney and Lohmeyer [6] demonstrate that dilutions of a factor of 30 occur in practice so that the effects of mixing may be expected to be important.

Examination of the available experimental data shows an aspect ratio of unity for gaseous experiments, and a range of values, generally smaller for aqueous experiments. Thus, an explanation of the low dilutions of aqueous experimental data and the high dilutions of gaseous experimental data may be the effects of the role of the aspect ratio. The influence of the aspect ratio, $h_0/2R_0$, is to make available a greater magnitude of potential energy for a high aspect ratio release in comparison to a lower aspect ratio release of equal volume. Thus it may be expected that mixing which arises from the release of this disturbing potential energy density is also dependent upon the aspect ratio.

Consider the radially contained volume Q_0 of dense fluid overlain by lighter, homogeneous fluid as illustrated in Fig. 1; after the removal of the containing lock gate,

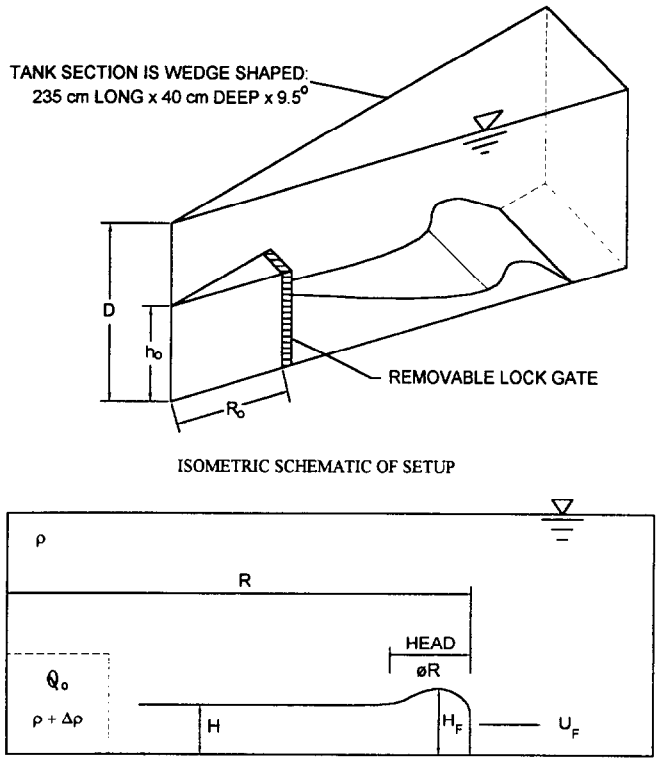

Fig. 1. Experimental configuration and definitions.

propagation arises because of the out of balance pressure forces (neglecting mixing, and assuming hydrostatic pressure distribution). The evolution of the leading edge is dependent on the reduced gravitational acceleration g' and the vertical scale H_F of the leading edge of the intrusion. This is described by

$$\frac{dR}{dt} = \lambda(g'H)^{\frac{1}{2}} \tag{1}$$

a result established by von Karman [14] and Benjamin [7]. The value of the constant λ, which is determined empirically, is in the range 1–1.2 (Fannelop and Waldman [15], Rottman and Simpson [2].

It is useful to consider a "box model" or similarity analysis (Fay [11], Fannelop and Waldman [15], Huppert and Simpson [1]). This widely used approach relies on the simplification that the current depth H is independent of distance R. For small times, or distances close to the vicinity of the containment vessel, the depth of the current is governed by the details of the initial conditions and so it is likely to evolve in a manner

dependent on the initial conditions. The box model approach is thus most valid for large times or distances from the release. Conservation of buoyancy requires

$$(g'H)\pi R^2 = g'_{that_0} \tag{2}$$

where g'_0 is the initial value of the reduced gravitational acceleration. The ratio of the initial volume to the volume of the gravity current after the removal of the lock gate gives the mean concentration $\overline{C}$

$$\overline{C} = \frac{Q_0}{\pi R^2 H} \tag{3}$$

Rearranging Eq. (2) and integrating Eq. (1) yields

$$(g'H) = at^{-1} \tag{4}$$

where $a = (g'_0 Q_0/4\pi)^{1/2}$. Substitution of Eq. (4) in Eq. (1) with $H = H_F$ shows that U_F, the velocity of propagation of the head, is described by

$$U_F = \frac{\mathrm{d}R}{\mathrm{d}t} = \lambda a^{1/2} t^{-1/2} \tag{5}$$

So that the growth of the gravity current after the removal of the lock gate is

$$R^2 = 4\lambda^2 at \tag{6}$$

a result first derived by Fay [11,16]. Observation suggests that entrainment occurs mainly at the head (Britter and Simpson[8,10]). An explicit form of the entrainment velocity U_E is facilitated by introduction of the parameter ϕ which is defined as the ratio of the local horizontal length of the head to the radius of the leading edge of the head. This is a measure of the relative entraining area of the gravity current. The visualizations of Britter and Simpson [8,10] and Huppert and Simpson [1] and present visualizations show clearly that $\phi < 1$ and that the head is annular. The rate of change of volume of the expanding radial gravity current is given by the rate of change of volume for a cylinder $(\frac{\mathrm{d}}{\mathrm{d}t}(\pi R^2 H)$. Assuming that entrainment U_E occurs at the head which is an annulus of length ϕR (and consequently an area $\pi(2\phi - \phi^2) R^2$) yields that the rate of change of volume is

$$\frac{\mathrm{d}}{\mathrm{d}t}(\pi R^2 H) = \pi(2\phi - \phi^2) R^2 U_E \tag{7}$$

which after some rearranging, yields

$$U_E = \left(\frac{Q_0}{\pi g'_0}\right)^{\frac{1}{2}} \frac{1}{2\lambda t \overline{C}(2\phi - \phi^2)} \frac{\mathrm{d}\overline{C}}{\mathrm{d}t} \tag{8}$$

With $\phi(t)$ and $\overline{C}(t)$ determined from experiments, Eq. (8) gives the value of the entrainment velocity U_E. The physical interpretation of Eq. (7) and Eq. (8) is simply that the rate of change of volume is due to an entrainment velocity U_E occurring uniformly over the extent of the head, which has a length ϕR. Note that the role of the aspect ratio appears indirectly in Eq. (8) as it is implicit in the term $\mathrm{d}\overline{C}/\mathrm{d}t$.

In terms of initial variables of the flow configuration (see Fig. 1), and understanding that $R = \frac{U_F H_F}{\nu} \gg 1$ and $P_E = \frac{U_F H_F}{K} \gg 1$ so that molecular effects are negligible, the length and time scales of the problem are $Q_0^{1/3}$ and $(Q_0^{1/3}/g_0')^{\frac{1}{2}}$. These scales are used to non-dimensionalize length and time in the presentation of the results which follow. Also the evolution of instantaneous finite volume releases of dense fluid is dependent on the non-dimensional groups $h_0/2R_0$ and h_0/D which are the aspect ratio and fractional depth respectively.

3. Experimental set-up

The experiments were conducted in a 235 cm long × 40 cm deep × 9.5° sector-shaped tunnel constructed of 1.25 cm thick plexiglass. An aluminum gate was located at $R = 32.5$ cm for high aspect ratio runs, and at $R = 60$ cm for low aspect ratio runs: the gate, which was greased, was removable almost instantaneously with little disturbance to the water column.

Although an exploratory series of experiments were conducted with heat as the buoyancy inducing agent, in all the experiments reported here the buoyancy was effected by dissolved cooking salt. Blue vegetable dye was added to the dense fluid for flow visualization. The initial density of the dense fluid was measured by hydrometers which are accurate to 0.02%. The dilution, defined as $\pi R^2 H/Q_0$ the inverse of Eq. (3), occurring during the experiment was determined by comparing the volume of the dyed gravity current from photographs to its known initial volume Q_0. This gives a bulk dilution which was verified by hydrometer measurements of selectively withdrawn fluid during preliminary runs.

The experimental procedure was to fill quickly with brine and fresh water on the appropriate sides of the gate to the desired value of h_0. Then fresh water was introduced to both sides very slowly to minimize mixing and so maintain a sharp interface. It took 2 hours to fill the tunnel to the required depth of 40 cm. Typical values of the interface thickness were 1 cm.

The experiment comprised of removing the lock gate instantaneously (it took less than 0.1 s). The leading edge of the developing gravity current was electronically timed to within 0.1 s, and the experiment photographed by a 35 mm camera and a 35 mm lens with 1/60 s exposures taken at approximately every 3 s. A 20 cm × 10 cm grid was marked to the side of the tunnel and facilitated scaling to within 1 mm on subsequently developed photographs.

Two series of experiments were conducted. The first series of eight runs with aspect ratio varying from 0.04–0.62 were all done with values of $g_0' \approx 10$ cm s^{-2}. A second series of five runs with aspect ratio varying from 0.14–0.62 were undertaken for larger values of reduced gravitational acceleration with $g_0' \approx 35$ cm s^{-2} and 100 cm s^{-2}. The run parameters are listed in Table 1.

Except for run L4 where viscous effects predominated in the final stages as determined by a $R \sim t^{1/8}$ growth rate (Huppert and Simpson [1]), the parameters are such that in all the runs inertial effects dominate. Reynolds numbers $U_F H_F/\nu$, defined by the velocity and depth of the head, typically were greater than 2000: Peclet numbers

Table 1
Run parameters

Run No.	D cm	R_0 cm	h_0 cm	$h_0/2R_0$	h_0/D	g'_0 cm s^{-2}	Q_0 cm^3	$Q_0^{1/3}$ cm	T s
L1	40	32.5	22.4	0.35	0.56	9.61	74,330	42.03	2.091
L2	40	32.5	31	0.48	0.78	9.03	102,866	46.84	2.278
L3	40	32.5	40	0.62	1.00	9.32	132,732	50.99	2.340
L4	40	60	5.1	0.04	0.13	8.83	57,680	38.62	4.374
L5	40	60	28.5	0.24	0.71	9.96	322,340	68.56	2.624
L6	40	60	25	0.22	0.63	9.81	282,744	65.63	2.587
L7	40	60	20.5	0.17	0.51	10.79	231,850	61.43	2.386
L8	40	60	9	0.08	0.23	10.40	101,776	46.69	2.119
M1	40	32.5	29.3	0.45	0.73	34.83	97,226	45.97	1.149
H	40	32.5	40	0.62	1.00	98.1	132,573	50.99	0.721
2H	40	32.5	26	0.40	0.65	97.1	89,135	44.67	0.678
3H	40	32.5	16.9	0.26	0.43	96.1	55,699	38.19	0.630
4H	40	60	13.5	0.11	0.33	99.5	153,130	53.47	0.733

Notes: $Q_0 = \pi R_0^2 h_0$ and because the tank is a 9.5° sector, Q_0 is $360/9.5 \approx 38$ times the actual amount in the experiment. $T = (Q_0^{1/3}/g'_0)^{\frac{1}{2}}$.

$U_F H_F/K$ were greater than 10^6 where K is the diffusivity of salt in water. A limitation of the present experiment is that it is difficult to attain high values of aspect ratio with small values of fractional depth. This is because of significant viscous effects for small fractional depths ≤ 0.2 for the scales of this experiment.

4. Results

4.1. Visual observations

Immediately after the removal of the gate the dense fluid column collapses. The form of the collapse is complex and varied. Multiple fronts formed for configurations whose initial fractional depth (h_0/D) exceeded 0.5. Fig. 2 shows a series of sequential visualizations of the typical evolution of the flow after an instantaneous release for a relatively large value of the fractional depth. Multiple fronts, comprising vortices of height of approximately half of the initial depth of the dense fluid h_0, arise from the initial roll-up of dense fluid after release. Such multiple fronts persist up to a time $t^* = t/T \sim 3$ where T is defined as $(Q_0^{1/3}/g'_0)^{\frac{1}{2}}$. The evolution for a typical release with a low value of fractional depth of Fig. 3 reveals that the structure is similar to the steady-state gravity currents described by Britter and Simpson [8,9] in that there is a single front or head. For releases of all values of fractional depth the structure evolves to a single head for large times $t^* > 6$. The sequential visualizations of Figs. 2 and 3 show that the bulk of the dense fluid is concentrated in a vortex-ring at the leading edge of the intrusion: the edge of the vortex-ring is irregular with lobes and clefts predominant. This region, the head, is deeper and seems qualitatively different from the following flow, in particular intense turbulent motions indicative of mixing were seen to be limited to the head. This is in keeping with the assumption made in the box model analysis (Eq. (7) and Eq. (8)) that entrainment occurs primarily at the head.

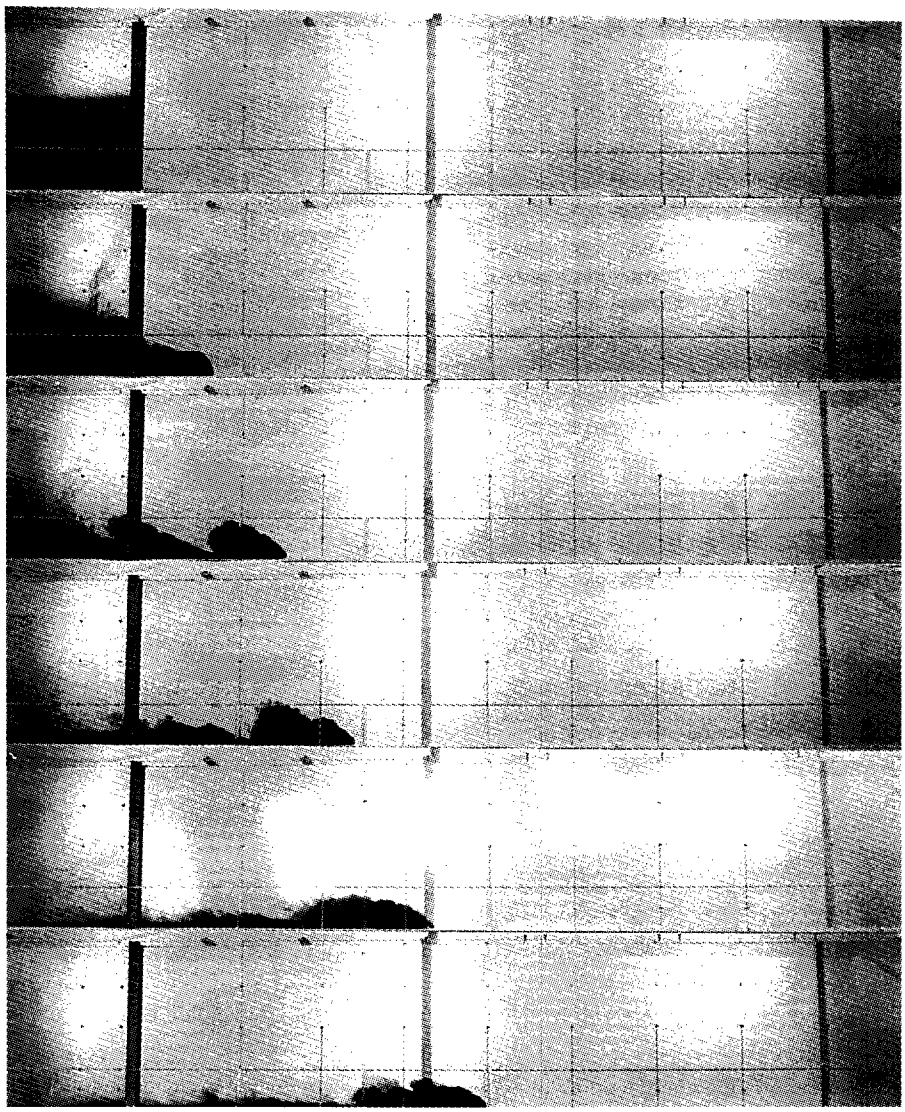

Fig. 2. The sequential visualization of evolution of flow after instantaneous release. Visualization is for run L1 whose aspect ratio is 0.35 and fractional depth $h_0/D = 0.56$. See Table 1 for run parameters. From top to bottom visualization times are: 0; 1.2; 3.9; 6.8; 10.1 and 13.1 s. Note the appearance of multiple fronts at 3.9 s, and their degeneration by 6.8 s. Vertical lines are spaced 20 cm apart. $T = 2.09$ s.

4.2. Growth rate, dilution and entrainment rates

The effect of aspect ratio on the evolution of the intrusion were determined by detailed analysis of (sequential) visualizations. The growth of the intrusion is shown in Fig. 4. Here the ordinate is the source of the non-dimensional radius $R^* = (R -$

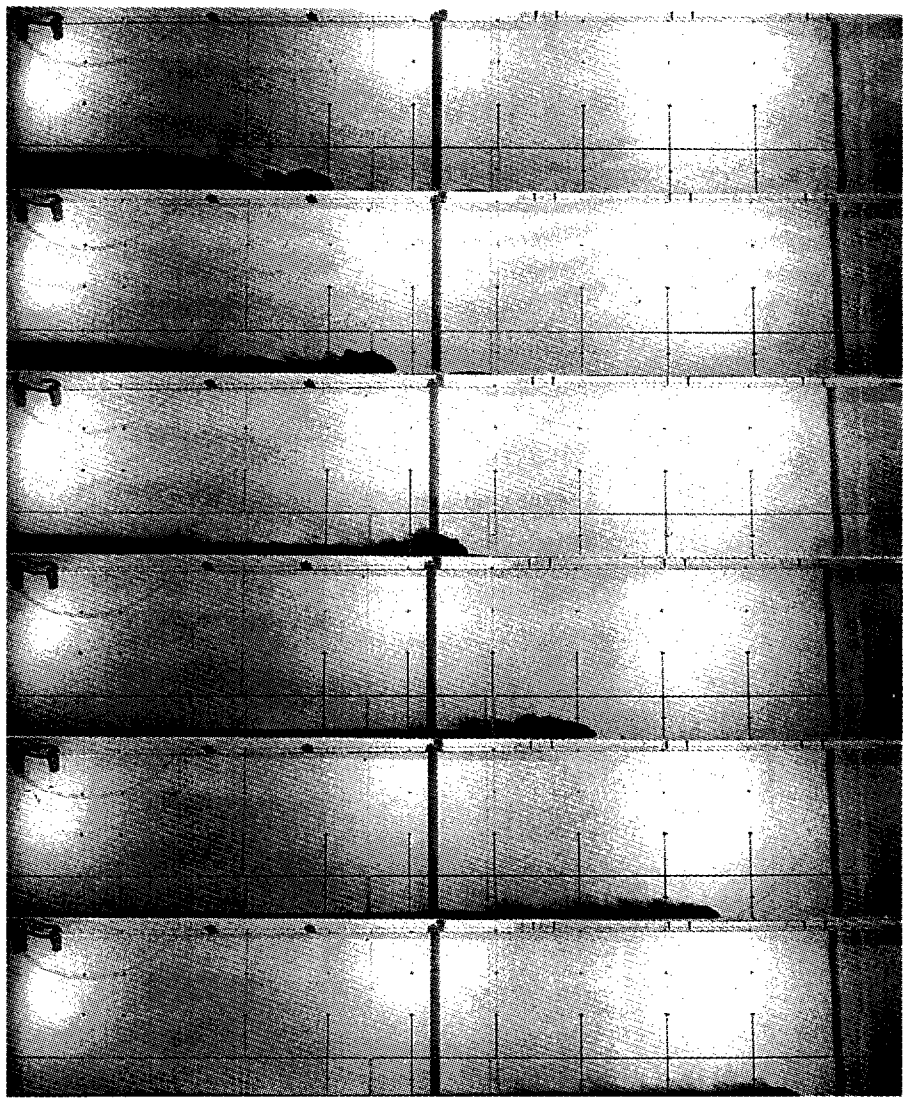

Fig. 3. The sequential visualization of flow for run L8 whose aspect ratio is 0.08 and fractional depth is 0.23. See Table 1 for run parameters. From top to bottom times of visualization are: 1.5; 4.1; 7.7; 14.4; 21.8; 27.5 s. $T = 2.119$ s.

$R_0)/Q_0^{1/3}$, where R_0 is the radius of the location of the gate. The intrusion grows from $R^{*2} \approx 2$ at $t^* \approx 3$ to $R^{*2} \approx 25$ at $t^* \approx 25$. The $R^2 \sim t$ prediction of the box model (Eq. (6)) is asymptotically approached. For small times the box model is not valid; for large times $t^* > 10$ the data clearly follow the predictions of a $+1$ slope. The data is in agreement with the results of gaseous experiments of Spicer and Havens [5]: the data indicates a value of $\lambda = 1.12$ in Eq. (5) and Eq. (6) of the box model for $t^* > 10$.

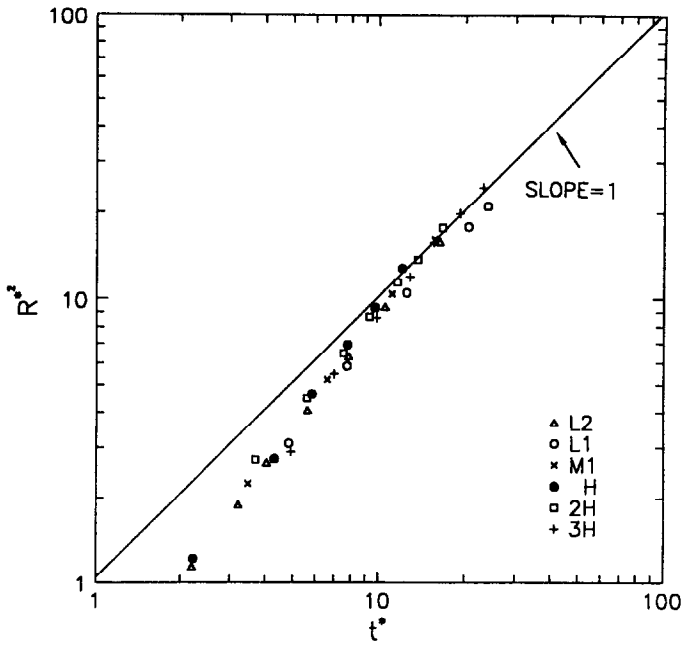

Fig. 4. The non-dimensional growth rate of cloud. A line of slope +1 through the data is shown. $R^* = (R - R_0)/Q_0^{1/3}$.

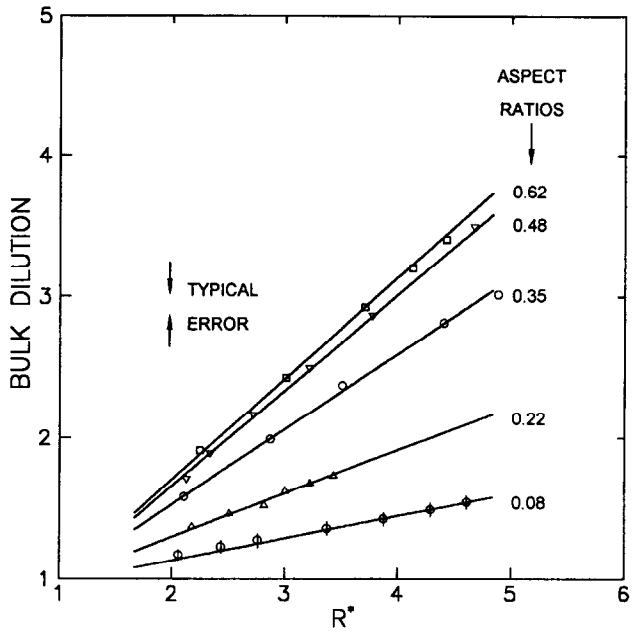

Fig. 5. The variation of dilution with non-dimensional distance and aspect ratio. Lines are the best fit through data. Data for $g_0') = 10$ cm s^{-2}.

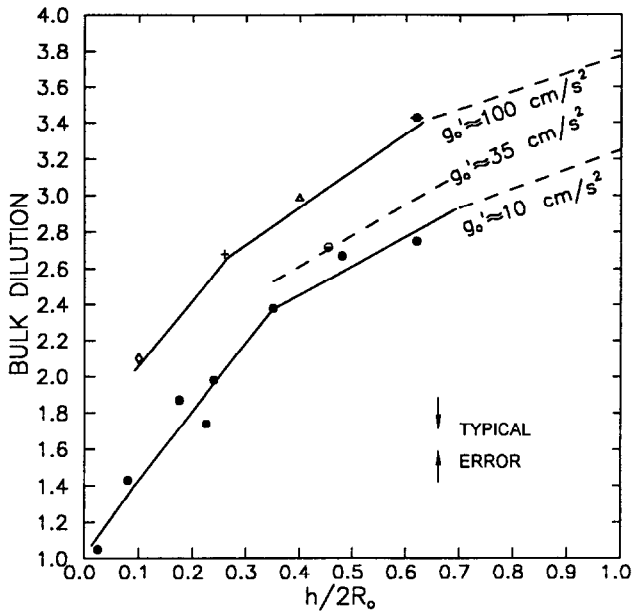

Fig. 6. The increase of dilution with aspect ratio at $R^* = 3.5$. Data for $g_0' = 10, 35, 100$ cm s^{-2}.

Fig. 5 shows that dilutions increase linearly with distance for all values of aspect ratios (at least up to $R^* \sim 5$). For example, for a release with aspect ratio equal to 0.35 at $R^* = 2.2$, dilution = 1.6 whereas at $R^* = 4.9$, dilution = 3. Also evident is a systematic variation of dilution with aspect ratio with greater dilutions for larger values of the aspect ratio.

The increase in dilution with increasing aspect ratio is shown explicitly in Fig. 6. There is a 100% increase in dilution for the data of $g_0' = 10$ cm s^{-2} at $R^* = 3.5$ as the aspect ratio is increased from 0.1 to 0.6. The data suggests that the rate of increase of dilution is greatest for aspect ratios less than 0.3, with decreasing rates of increase of dilution for higher aspect ratios.

There also appears to be a small dependence upon the value of g_0' which suggests non-Boussinesq effects for larger values of $\Delta\bar{\rho}/\bar{\rho}$. For example, the data for $g_0' = 100$ cm s^{-2} shows greater values of dilution than for $g_0' = 10$ cm/s^2; however, the rate of increase of dilution for $g_0' = 100$ cm s^{-2} are smaller than for $g_0' = 10$ cm s^{-2} in that there is 29% increase in dilution for data of $g_0' = 100$ cm s^{-2} between aspect ratios of 0.25 and 0.6 whereas there is a 41% increase in dilution for $g_0' = 10$ cm s^{-2}.

A caveat is that in assessing dilution and entrainment rates it should be noted that for runs with high values of the initial fractional depth ($h_o/D > 0.8$, see Table 1) a counter-flowing gravity current forms near the surface (Rottman and Simpson [2]). This increases the effective interfacial shear on the evolving (bottom) intrusion. It is difficult to assess the consequence of this shear on values of dilution but as Fay [16] has shown that entrainment velocity U_E is not governed by local shear, any effect is likely to be

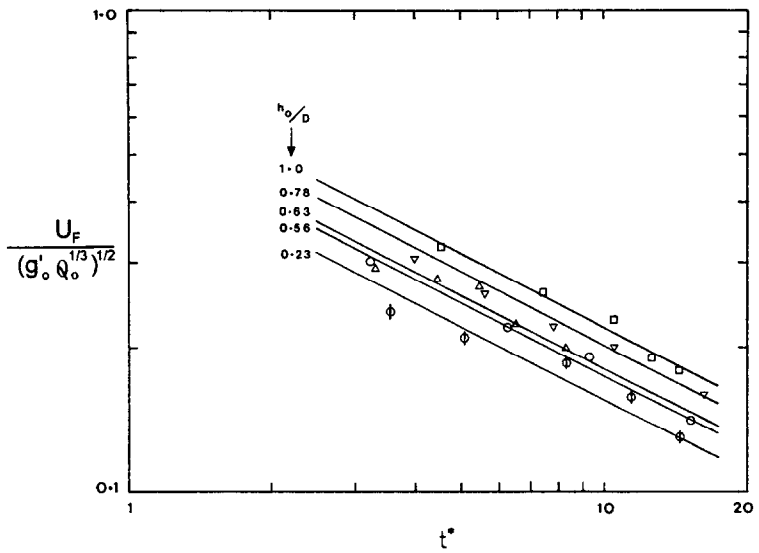

Fig. 7. The dependence of non-dimensional front velocity on fractional depth h_0/D. Best fit lines of slope $-1/2$ are shown for data of various values of h_0/D. Data for $g'_0 = 10$ cm s^{-2}.

small. This is because entrainment is principally driven by the evolving vortex structure created by the initial roll-up after release (see visualizations of Figs. 2 and 3).

Velocities of the front (i.e., the leading edge of the head region) are shown in Fig. 7. Here the ordinate is the non-dimensional front velocity $U_F/(g'_0 Q_0^{1/3})^{\frac{1}{2}}$. The data indicates a trend for larger front velocities for larger values of fractional depth h_0/D; at $t^* \approx 5$, $U_F/(g'_0 Q_0^{1/3}) \approx 0.31$ and 0.21 for $h_0/D = 1.0$ and 0.23 respectively. Clearly front velocities also decay with time. Best fit lines of slope $-1/2$ have been drawn through the data for each value of the fractional depth: as can be seen the agreement with the prediction of Eq. (6) of $U_F \sim t^{-1/2}$ is good for all fractional depths.

Entrainment velocities U_E were determined by calculating the volume of the intrusion and the head length from visualizations at successive times (see Eq. (8)). Similar to the evolution of the front velocity U_F entrainment velocities were also found to decrease in time. The evolution of non-dimensional entrainment velocity, $U_E/(g'_0 Q_0^{1/3})^{\frac{1}{2}}$ for data for various values of aspect ratio is shown on Fig. 8. The data shows that the influence of the aspect ratio is profound initially. For example at $T^* \sim 3$ the non-dimensional entrainment rate is an order of magnitude greater for aspect ratio of 0.62 in comparison with entrainment rates for aspect ratio of 0.08. Subsequently the influence of the aspect ratio diminishes as is shown by the convergence of the best fit lines of non-dimensional entrainment velocities for various values of aspect ratio drawn through the data. The data suggests that the effect of the aspect ratio may be expected to be indistinguishable for large times ($T^* > 50$).

A useful deduction can be made by comparing the slopes of the non-dimensional entrainment velocity best fit lines with the best fit line of the non-dimensional front velocity in Fig. 8. For the low aspect ratio run of $h/2R_0 = 0.08$, the slope of the

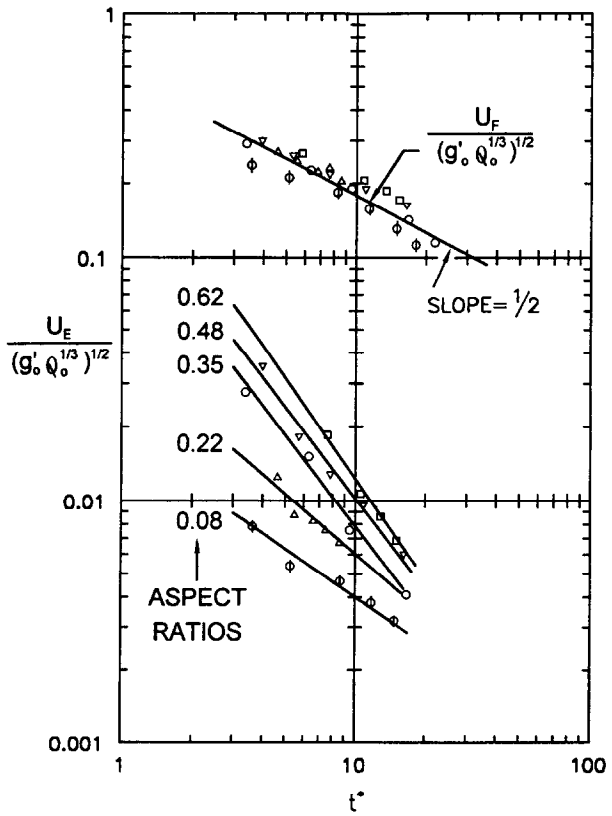

Fig. 8. Variation of non-dimensional front and entrainment velocity with non-dimensional time and aspect ratio. Note that the best fit line through front velocity data has a $-1/2$ slope. Data for $g'_0 = 10$ cm s^{-2}.

entrainment velocity data is approximately the same ($\approx -1/2$) as the slope of the front velocity data so that it may be inferred that entrainment velocity is proportional to the front velocity ($U_E/U_F = 0.02$ approximately). This is similar to the steady state gravity current experiments of Britter and Simpson [8] who also found that entrainment velocity was proportional to the front velocity. Large value aspect ratio releases results in intrusions with very large initial rates of entrainment, and whose entrainment velocities are not simply proportional to the front velocity (e.g., for an aspect ratio of 0.62 at $t^* \approx 5, U_E/U_F = 0.13$ whereas at $t^* \approx 15$, $U_E/U_F \approx 0.05$).

5. Conclusions

A study of the dilution arising from the instantaneous release of relatively dense, axisymmetric, finite volumes in water has been conducted. The initial form of the collapse of the dense fluid was complex and varied, multiple fronts which degenerate to a single front, formed for configurations with large initial fractional depths (h_0/D). The

structures of the subsequent flow field in all cases was observed to consist of a region (the head) of intense motions, indicative of mixing, which was deeper than the following flow. Analysis showed that the leading edge of the head grew in time as $R^{*2} \sim t^*$, and that values of dilution grew linearly with distance R^*. Dilutions were also found to vary with aspect ratio $(h_0/2R_0)$ with large dilutions for large aspect ratios. The propagation velocity of the head $U_F/(g'_0 Q_0^{1/3})^{\frac{1}{2}}$ was found to decrease as $t^{*-1/2}$: entrainment velocities $U_E/(g'_0 Q_0^{1/3})^{\frac{1}{2}}$ were also found to decrease with time, but the manner of the decrease varied with the aspect ratio. For low aspect ratio $(h_0/2R_0 < 0.1)$ entrainment velocities were proportional to the velocity of the head U_F (i.e., $U_E \sim U_F$ with the constant of proportionality being approximately 0.02).

For high aspect ratios entrainment velocities are much greater and do not vary with the velocity of the head in a simple proportional manner. The influence of the aspect ratio on entrainment velocity decreases with time, and extrapolation of the present results suggests that the dependence of the entrainment velocity on aspect ratio will be small for large times $t^* > 50$.

Acknowledgements

It is a pleasure to acknowledge informative discussions with Dr J.W. Rottman.

References

[1] H.E. Huppert and J.E. Simpson, J. Fluid Mech., 99 (1980) 785.
[2] J.W. Rottman, J.E. Simpson, J. Fluid Mech., 135 (1983) 95.
[3] D.J. Hall, Further experiments on a model of an escape of heavy gas, LR(312)AP, Warren Spring Laboratory (1979).
[4] D.J. Hall, E.J. Hollis and H. Ishaq, A wind tunnel model of the Porton dense gas spill field trials, LR(394)AP, Warren Spring Laboratory (1982).
[5] T.O. Spicer and J.A. Havens, J. Hazardous Mater., 11 (1985) 95.
[6] R.N. Meroney and A. Lohmeyer, Growth spreading and dispersion of dense gas clouds released suddenly into a turbulent boundary layer, GRL-81/0025, Gas Research Institute, Chicago.
[7] T.B. Benjamin, J. Fluid Mech., 31 (1968) 209.
[8] R.E. Britter and J.E. Simpson, J. Fluid Mech., 88 (1978) 223.
[9] J.E. Simpson, R.E. Britter, J. Fluid Mech., 94 (1979) 477.
[10] J.E. Simpson, R.E. Britter, J. Fluid Mech., 112 (1981) 459.
[11] J.A. Fay, The spread of oil slicks on a calm sea, in D.P. Hoult (Ed.), Oil on the Sea, Plenum (1969) 53–63.
[12] D.P. Hoult, Annual Review of Fluid Mech., 4 (1972) 341.
[13] J.W. Rottman, J.C.R. Hunt and A. Mercer, J. Hazardous Mater., 11 (1985) 261.
[14] T. von Karman, Bull. Amer. Math. Soc., 46 (1940) 615.
[15] T.K. Fannelop and G.D. Waldman, AIAA J, 10 (1972) 506.
[16] J.A. Fay, Experimental observation of entrainment rates in dense gas dispersion tests, in G. Ooms and H. Tennekes (Eds.) Atmospheric dispersion of heavy gases and small particles, Springer-Verlag, 1984, 39–51.